Silk fibroin/sodium alginate composite nano-fibrous scaffold prepared through thermally induced phase-separation (TIPS) method for biomedical applications

Haiping Zhang, Xiaotian Liu, Mingying Yang, Liangjun Zhu *

Institute of Applied Bioresources, College of Animal Sciences, Zhejiang University, Hangzhou 310058, Zhejiang, China

ARTICLE INFO

Article history:
Received 18 October 2014
Received in revised form 25 March 2015
Accepted 16 May 2015
Available online 21 May 2015

Keywords:
Silk fibroin
Sodium alginate
Nano-fibrous
Cell biocompatibility

ABSTRACT

To mimic the natural fibrous structure of the tissue extracellular matrix, a nano-fibrous silk fibroin (SF)/sodium alginate (SA) composite scaffold was fabricated by a thermally-induced phase-separation method. The effects of SF/SA ratio on the structure and the porosity of the composite scaffolds were examined. Scanning electron microscopy and porosity results showed that the 5SF/1SA and 3SF/1SA scaffolds possessed an excellent nano-fibrous structure and a porosity of more than 90%. Fourier transform infrared, X-ray diffraction, and differential scanning calorimetry results indicated the physical interaction between SF and SA molecules and their good compatibility in the 5SF/1SA and 3SF/1SA scaffolds, whereas they showed less compatibility in the 1SF/1SA scaffold. Cell culture results showed that MG-63 cells can attach and grow well on the surface of the SF/SA scaffolds. The nano-fibrous SF/SA scaffold can be potentially used in tissue engineering.

1. Introduction

Scaffold biomaterials can provide synthetic three-dimensional templates similar to natural extracellular matrix environments for tissue regeneration [1]. An ideal scaffold for tissue engineering and regenerative medicine should have the following characteristics: (1) an extensive network of interconnecting pores so that cells can migrate, multiply, and attach deep within the scaffolds; (2) a high surface area to facilitate cell seeding, adhesion, and proliferation; (3) a proper degradation rate to match the rate of new tissue formation; and (4) biocompatibility with a high affinity for cells to attach and proliferate [2,3]. Nano-fiber scaffolds in particular have become a hotspot in the field of tissue engineering for their high porosity, large surface area, and regulatable mechanical properties, as well as their similarities to the structure of natural extracellular matrices [4,5].

Considerable efforts have been made in recent years to create nano-fibrous scaffolds by various methods, including electrospinning, self-assembly, and thermally induced phase separation (TIPS) [6–8]. The

2. Materials and methods

2.1. Materials

Silk cocoons were obtained from Huzhou Fiber Inspection (Huzhou, China). SA was purchased from Sinopharm Chemical Reagent Co., Ltd. 1,4-Dioxane was purchased from Aladdin Co., Ltd. All other chemicals and solvents used were analytical grade.

2.2. Preparation of SF aqueous solution and SA aqueous solution

Silk cocoons were degummed by treating them twice with a 5 g/L sodium carbonate water solution at 98 °C for 30 min and washing with deionized water several times to remove sericin from the silk fibers. The degummed fibers were dissolved in 9.3 M LiBr at 37 °C for 6 h to obtain the regenerated SF solution after being dried completely. The obtained SF solution was then dialyzed against deionized water for 4 days with several changes to remove the LiBr molecules. The concentration of the dialyzed pure regenerated SF solution was adjusted to 5%. SA was dissolved in deionized water at 60 °C and its concentration was 0.5%.

2.3. Fabrication of scaffolds

SF/SA composite scaffolds with SF/SA weight ratios 5:1; 3:1, and 1:1 were prepared with the TIPS method as follows: The SF solution was first fully stirred with the SA solution at 60 °C to obtain an SF/SA blend aqueous solution. The 1,4-dioxane/water (9:1, w/v) solvent was then homogeneously mixed with it. The volume ratio of the 1,4-dioxane/water solvent to the SF/SA blend solution was set at 1:3. The SF/SA/1,4-dioxane/water mixtures were then dropped into a 24-well cell culture plate and rapidly transferred into a container at −80 °C for 4 h to induce the gel formation. Then the gel was thawed at room temperature and immersed into cold ethanol (−20 °C) for 24 h to solidify the gel. The wet SF/SA scaffold was obtained by washing the solidified gel with deionized water to remove the ethanol and the 1,4-dioxane and then freeze-drying it for 24 h for further characterization. The detailed experimental procedure for the SF/SA composite scaffold is illustrated in Fig. 1. Pure SF and SA scaffolds were also prepared with the above method as the controls.

2.4. Characterization

2.4.1. Scanning electron microscopy (SEM)

The scaffolds were sputter-coated with gold and then observed with scanning electron microscopy with an accelerating voltage of 10 kV (SEM, Philips XL30, The Netherlands).

2.4.2. FTIR spectroscopy

An FT-IR-8400S infrared spectrometer (SHIMADZU, Japan) was used to collect the FTIR spectrum of the scaffolds between 4000 and 400 cm^{-1} with the KBr pellet technique. The resolution and the scanning times was 4 cm^{-1} and 40, respectively.

2.4.3. X-ray diffraction (XRD)

X-ray diffraction patterns were collected on an X-ray diffractometer (PaNalytical, The Netherlands) with Cu Kα and the irradiation conditions were 40 kV and 40 mA. The 2θ scanning ranged between 5° and 80° with a step scanning rate of 2°/min.

2.4.4. Differential scanning calorimetry (DSC)

The thermal behavior of the scaffolds was determined using a DSC822e differential scanning calorimeter (Mettler Toledo, Holland). The measurements were carried out in the range of 30–450 °C under nitrogen at a scanning rate of 10 °C/min.

2.4.5. Porosity

The porosity of the scaffolds was measured by the liquid displacement test. The scaffolds were immersed into a known volume (V_1) of ethanol in a graduated cylinder for 5 min. Then repeated vacuumization was done until no bubble emissi. o 4 s w 7 (a) 0 (9 (i) 0

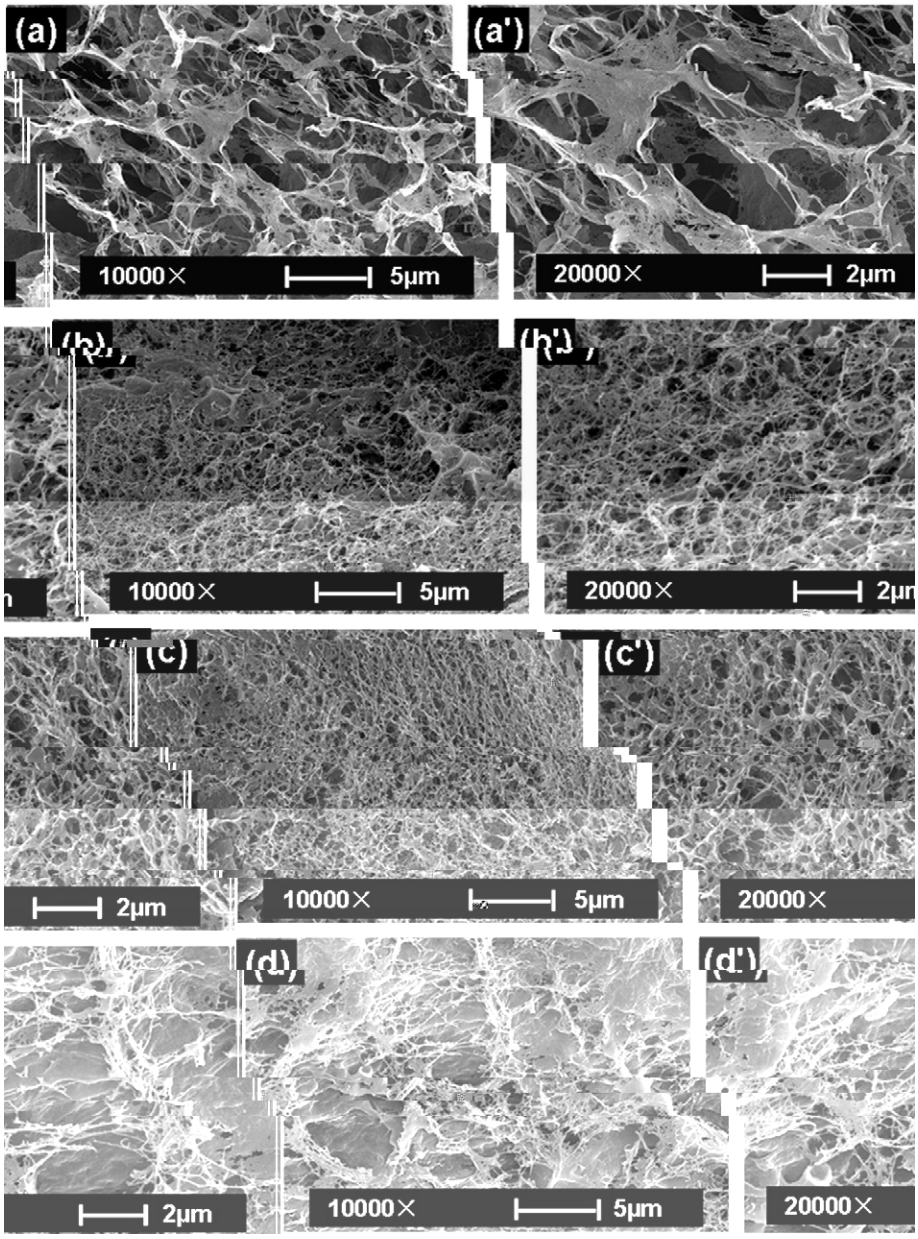

Fig. 2. SEM micrographs of the scaffolds prepared through TIPS method. (a) and (a′): SF, (b) and (b′): 5SF/1SA, (c) and (c′): 3SF/1SA, and (d) and (d′): 1SF/1SA. The magnification of (a)–(d) was 10,000× and (a′)–(d′) was 20,000×.

2.5. Cell morphology and viability

2.5.1. Cell culture

MG-63 osteoblasts were cultured in High Dulbecco's Modified Eagle Medium (H-DMEM, Cibco, USA) supplemented with 10% fetal bovine serum (FBS, PAA, Germany), 100 IU/mL of penicillin (Sigma, USA), and 100 mg/mL of streptomycin (Sigma, USA) in a CO_2 incubator at 37 °C with 5% CO_2 and saturated humidity. The scaffolds were cut into circular discs, each with a diameter of 6 mm and a height of 2 mm, and put into 96-well tissue culture plate wells. The scaffold samples were sterilized with 75% alcohol for 2 h, rinsed twice with phosphate buffer saline (PBS), and soaked in culture medium for 12 h before cell culturing. Each scaffold was seeded with 5×10^4 cells.

2.5.2. Cell morphology

SEM was used to determine the morphology of the cells seeded on the scaffolds. After culturing for 7 days, the seeded scaffolds were immediately rinsed with PBS (pH 7.4), and fixed with 3% glutaraldehyde overnight at 4 °C. The fixed samples were then dehydrated with a gradient of ethanol and washed with PBS, and later fixed with 1% osmium acid at 4 °C and dried with the critical-point drying method. After being sputter-coated with an ultrathin gold layer, samples were observed by SEM.

2.5.3. MTS assay

The cell proliferation rate was examined by methoxyphenyl tetrazolium salt (MTS) assay with 3-(4,5-dimethyl-thiazol-2-yl)-5-(3-carboxymethoxyphenyl)-2-(4-sulfophenyl)-2H-tetrazolium (MTS, Promega, USA) for mitochondrial reduction. The quantity of the formazan product, measured by the absorbance at 490 nm using a microplate reader, is directly proportional to the number of living cells in the culture. The scaffolds were sterilized with ethanol for 2 h and washed with PBS several times to remove the residual ethanol before being placed in a 96-well plate. MG-63 cells were seeded at a density of 5×10^4 cell/mL in a 200 μL DMEM culture medium

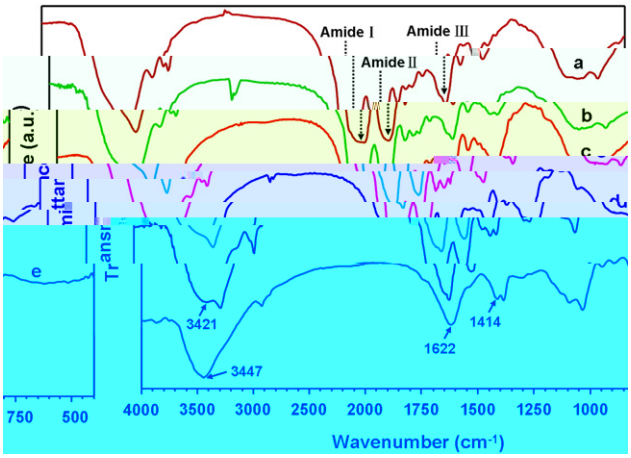

Fig. 3. FTIR spectra of the scaffolds prepared through TIPS method. (a) SF, (b) 5SF/1SA, (c) 3SF/1SA, (d) 1SF/1SA, and (e) SA.

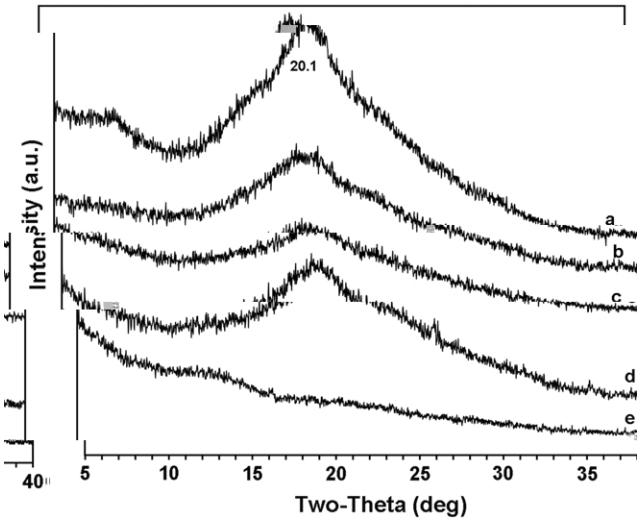

Fig. 4. XRD patterns of the scaffolds prepared through TIPS method. (a) SF, (b) 5SF/1SA, (c) 3SF/1SA, (d) 1SF/1SA, and (e) SA.

supplemented with 10% fetal bovine serum. After culturing the cells under 5% CO_2 at 37 °C for 1, 3, and 7 days, 50 μL of the MTS solution was added to each well and incubated for 4 h. Cells cultured in the 96-well plate without scaffolds were tested as blanks. The experiment was repeated three times and the results are presented as mean ± standard deviation (SD). One-way analysis of variance (ANOVA) was conducted. The difference of statistical results was considered significant when $p < 0.05$ (labeled with one asterisk) and as extremely significant when $p < 0.01$ (labeled with a double asterisk).

3. Results and discussion

3.1. Scaffold characterization

3.1.1. Scaffold morphology

The cross-sectional SEM micrographs of pure SF, 5SF/1SA, 3SF/1SA, and 1SF/1SA scaffolds prepared through the TIPS method are shown in Fig. 2. The pure SA scaffold is not shown because of the difficulty of integrally separating it from the mold. The SF scaffold showed an interconnected porous morphology with large pore size (Fig. 2a and a′). After being mixed with SA, the scaffolds became more flexible and spongy (Fig. 1) and showed a three-dimensional (3D) nano-fibrous porous structure with fiber diameters of 50–500 nm (Fig. 2b–d and b′–d′), which is obviously different from the SF scaffold. The results indicated that the introduction of SA into the SF scaffold can promote the formation of a nano-fibrous structure.

The samples of 5SF/1SA (Fig. 2b and b′) and 3SF/1SA (Fig. 2c and c′) showed a similar uniform nano-fibrous porous structure. Although many nano-fibers can also be observed in the 1SF/1SA scaffold (Fig. 2d and d′), a large amount of non-fibrous and non-porous aggregates were observed. Therefore, too much SA in the composite scaffold is not advantageous to the formation of a nano-fibrous structure. This may result from the excellent interaction and compatibility of SF and SA in the 5SF/1SA and 3SF/1SA scaffolds, but they are less compatible in the 1SF/1SA scaffold for the partial phase separation.

Table 1
Characteristic FTIR peaks of the scaffolds prepared through TIPS method.

Samples	Amide I	Amide II	Amide III	Stretching vibration of O–H group	Asymmetric stretching of $-COO^-$	Symmetric stretching of $-COO^-$
SF	1630	1522	1232	/	/	/
5SF/1SA	1628	1526	1236	3421	/	1412
3SF/1SA	1628	1526	1236	3421	/	1412
1SF/1SA	1628	1526	1236	3421	/	1412
SA	/	/	/	3447	1622	1414

3.1.2. FTIR analysis

To confirm the interaction of SF and SA in the composite scaffolds, FTIR analysis was conducted. The spectra of the scaffolds are shown in Fig. 3 and their characteristic peaks are listed in Table 1. Fig. 3a shows the FTIR spectrum of the SF scaffold. Its characteristic peaks occurred at 1630 cm^{-1} (amide I), 1522 cm^{-1} (amide II), and 1232 cm^{-1} (amide III), which represent the β-sheet structure presumably induced during the ethanol treatment [23,24]. From the spectrum of the SA scaffold, the characteristic peaks at 3447 cm^{-1}, 1622 cm^{-1}, and 1414 cm^{-1} correspond to the stretching vibration of the O–H group and the asymmetric and symmetric stretching vibrations of the COO^- group, respectively [25].

In the SF/SA composite scaffolds, the amide I peak of SF was overlapped with the asymmetric $-COO^-$ group stretching vibration of SA and was strengthened and somewhat shifted to 1628 cm^{-1}. The amide II and amide III peaks of SF increased somewhat to 1526 cm^{-1} and 1236 cm^{-1}, respectively, and their strengths obviously decreased in the 1SF/1SA scaffold with increasing SA. Furthermore, the stretching vibration of the O–H group and the symmetric stretching vibration of the COO^- group of SA decreased to 3421 cm^{-1} and 1412 cm^{-1},

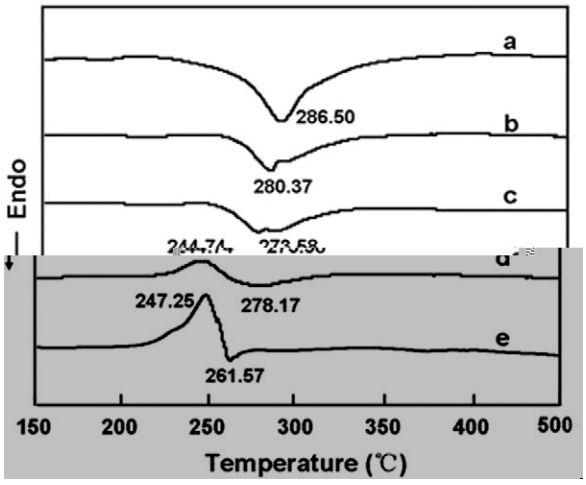

Fig. 5. DSC curves of the scaffolds prepared through TIPS method. (a) SF, (b) 1SF/1SA, (c) 3SF/1SA, (d) 5SF/1SA, and (e) SA.

Table 2
Porosities of the scaffolds prepared through TIPS method.

Samples	Porosity (%)
SF	86.36 ± 4.07
5SF/1SA	92.74 ± 3.42
3SF/1SA	90.70 ± 2.39
1SF/1SA	87.12 ± 3.75

respectively, and their strength gradually increased with increasing SA amount. The peak shift results indicate that SF was combined with SA through physical bonds such as the electrostatic interaction between amino and COO^- groups and the hydrogen bonding [26].

3.1.3. XRD analysis

XRD was used to study the crystalline structure of the scaffolds, and the patterns are shown in Fig. 4. The diffraction peak of the SF scaffold was observed at $2\theta = 20.1°$ (Fig. 4a), denoting the β-sheet secondary structure [27,28]. The peak at $2\theta = 10°$ to 15° of the SA scaffold showed the typical amorphous structure of SA [25]. In all SF/SA scaffolds, a diffraction peak at $2\theta = 20.1°$ was observed, although the intensity of 3SF/1SA was lower than that of 5SF/1SA (Fig. 4b and c) because of a higher number of SF molecules interacted with SA molecules. However, the intensity of 1SF/1SA (Fig. 4d) was higher than that of 3SF/1SA, probably due to the partial phase separation of SF and SA, as shown in the SEM results, and the increase of the self-assembly among SF molecules.

3.1.4. DSC analysis

Fig. 5 shows the DSC curves of the scaffolds. The DSC curve of SF (Fig. 5a) exhibits an endothermic peak at 286.50 °C, corresponding to the decomposition peak of SF [29]. The sharp exothermic peak of SA at 247.25 °C is due to SA collapsing to a relatively stable intermediate, and the weak endothermic peak at 261.57 °C can be attributed to the decomposition of the intermediate (Fig. 5e) [30]. The endothermic peak of the 5SF/1SA and 3SF/1SA composite nano-fiber scaffolds shifts to lower temperatures with the increasing amount of SA as compared to the pure SF scaffold, and the exothermic peak of SA at 247.25 °C was not obviously observed. However, with the 1SF/1SA composite scaffold, the endothermic peak was observed at 278.17 °C, which is somewhat higher than that of the 3SF/1SA scaffold, and the exothermic peak of SA occurred at 244.74 °C. The results indicate the compatibly interaction between SF and SA through hydrogen bonding in the 5SF/1SA and 3SF/1SA scaffolds and the partial phase separation of SF and SA in the 1SF/1SA scaffold, which agrees with the SEM and XRD results.

3.1.5. Porosity analysis

The porosities of the scaffolds are listed in Table 2 and all scaffolds possessed high porosity (>85%). The high porosity of a scaffold can provide benefits for cell growth and migration [31]. As compared with other scaffold samples, the pure SF scaffold showed relatively lower porosity while having the larger size porous structure, as shown in the SEM results. The porosity of the 5SF/1SA scaffold increased, which is caused by the homogeneous nano-fibrous structure. With the decrease in the amount of SF in the composite SF/SA scaffolds, the porosity of the scaffolds gradually decreased, and that of the 1SF/1SA scaffold was the lowest for the less nano-fibrous structures (Fig. 2d and d′).

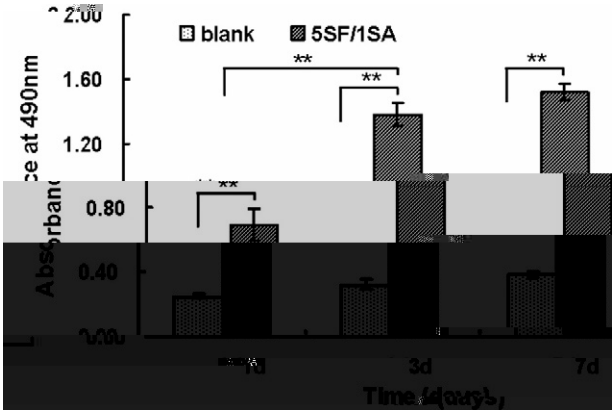

Fig. 7. Cell proliferation rates on the 5SF/1SA composite nano-fiber scaffolds after culturing for 1, 5, and 7 days.

3.2. Cell culture on the scaffolds

The cell biocompatibility of the 5SF/1SA scaffold was studied through SEM observation and the MTS assay method. Fig. 6 shows the morphology of MG-63 osteoblasts on the three SF/SA composite scaffolds prepared through the TIPS method after 7 days of culturing. The SEM results show that MG-63 osteoblasts can grow well on the surface of SF/SA composite scaffolds, with their tentacles close to the material surface. Because the 5SF/1SA scaffold showed an excellent fibrous structure and the highest porosity, its cell viabilities after culturing cells for 1, 3, and 7 days were further studied through MTS assay. The absorbance results of the 5SF/1SA scaffold shown in Fig. 7 indicate that the adhesion and growth amount of cells were both significantly higher than those of the blank plate wells. The above results indicate the good cell biocompatibility of the SF/SA scaffolds.

4. Conclusions

Nano-fibrous SF/SA composite scaffolds can be successfully fabricated through the TIPS method. The composite scaffolds possess good connectivity, uniform distribution of nano-fibers with diameters of 50–500 nm, and a porosity of more than 85%. The 5SF/1SA and 3SF/1SA scaffolds

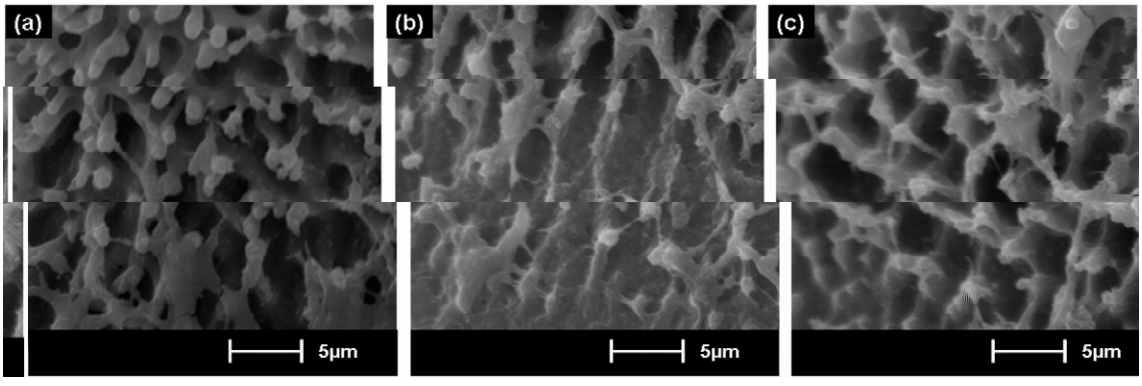

Fig. 6. The morphology of MG-63 osteoblasts on the SF/SA composite scaffolds prepared through TIPS method after 7 days of culturing. (a) 5SF/1SA, (b) 3SF/1SA, and (c) 1SF/1SA.

possessed excellent nano-fibrous structures and porosities higher than 90%, which is better than that of the 1SF/1SA scaffold. The characteristic peak shift results from FTIR analysis indicated physical interaction between the SF and SA molecules in the SF/SA scaffolds. The crystallinity strength and the thermal decomposition temperature changes further confirmed the interaction of the SF and SA molecules. SEM, XRD, and DSC results revealed good compatibility in the 5SF/1SA and 3SF/1SA scaffolds but less compatibility in the 1SF/1SA scaffold. MG-63 cell culture experiments confirmed the cell compatibility of the SF/SA scaffolds. These results promote the development and application of tissue engineering scaffold materials.

Acknowledgments

This work was supported by the National Natural Science Foundation of China (No. 31201855), the Zhejiang Leading Team of S&T Innovation (2011R50028), and the National Modern Agricultural Industry Technology System (CARS-22).

References

[1] P.X. Ma, Scaffolds for tissue fabrication, Mater. Today 5 (2004) 30–40.
[2] C. Liu, Z. Xia, J.T. Czernuszka, Design and development of three-dimensional scaffolds for tissue engineering, Chem. Eng. Res. Des. 7 (2007) 1051–1064.
[3] C.Y. Zhao, A. Tan, G. Pastorin, H.K. Ho, Nanomaterial scaffolds for stem cell proliferation and differentiation in tissue engineering, Biotechnol. Adv. 5 (2013) 654–668.
[4] G.B. Wei, P.X. Ma, Partially nanofibrous architecture of 3D tissue engineering scaffolds, Biomaterials 32 (2009) 6426–6434.
[5] J. Hu, K. Feng, X.H. Liu, P.X. Ma, Chondrogenic and osteogenic differentiations of human bone marrow-derived mesenchymal stem cells on a nanofibrous scaffold with designed pore network, Biomaterials 28 (2009) 5061–5067.
[6] Z.M. Huang, Y.Z. Zhang, M. Kotaki, et al., A review on polymer nanofibers by electrospinning and their applications in nanocomposites, Compos. Sci. Technol. 15 (2003) 2223–2253.
[7] L.W. Hamley, Self-assembly of amphiphilic peptides, Soft Matter 9 (2011) 4122–4138.
[8] J.H. Zhao, W.Q. Han, M. Tu, et al., Preparation and properties of biomimetic porous nanofibrous poly(L-lactide) scaffold with chitosan nanofiber network by a dual thermally induced phase separation technique, Mater. Sci. Eng. C-Mater. Biol. Appl. 32 (2012) 1496–1502.
[9] X.H. Liu, P.X. Ma, Phase separation, pore structure, and properties of nanofibrous gelatin scaffolds, Biomaterials 25 (2009) 4094–4103.
[10] J. Lannutti, D. Reneker, T. Ma, D. Tomasko, D. Farson, Electrospinning for tissue engineering scaffolds, Mater. Sci. Eng. C Mater. 3 (2007) 504–509.
[11] E. Beniash, J.D. Hartgerink, H. Storrie, S.I. Stupp, Self-assembling peptide amphiphile nanofiber matrices for cell entrapment, Acta Biomater. 4 (2005) 387